LETTERS

Mutual phase-locking of microwave spin torque nano-oscillators

Shehzaad Kaka[1], Matthew R. Pufall[1], William H. Rippard[1], Thomas J. Silva[1], Stephen E. Russek[1] & Jordan A. Katine[2]

The spin torque[1,2] effect that occurs in nanometre-scale magnetic multilayer devices can be used to generate steady-state microwave signals in response to a d.c. electrical current[3–8]. This establishes a new functionality for magneto-electronic structures that are more commonly used as magnetic field sensors and magnetic memory elements[9]. The microwave power emitted from a single spin torque nano-oscillator (STNO) is at present typically less than 1 nW. To achieve a more useful power level (on the order of microwatts), a device could consist of an array of phase coherent STNOs, in a manner analogous to arrays of Josephson junctions and larger semiconductor oscillators[10–12]. Here we show that two STNOs in close proximity mutually phase-lock—that is, they synchronize, which is a general tendency of interacting nonlinear oscillator systems[13–15]. The phase-locked state is distinct, characterized by a sudden narrowing of signal linewidth and an increase in power due to the coherence of the individual oscillators. Arrays of phase-locked STNOs could be used as nanometre-scale reference oscillators. Furthermore, phase control of array elements (phased array) could lead to nanometre-scale directional transmitters and receivers for wireless communications.

Mutually phase-locked interacting oscillators are surprisingly common natural occurrences. Examples of self-synchronizing systems include oscillations of interacting Josephson junctions[10,11,16,17], the rhythmic flashing of certain fireflies[18] and the oscillations of a system of two pendulum clocks coupled through a wall, as first reported by Huygens in the seventeenth century[19]. Participating elements of a phase-locked system must exhibit a nonlinear response to forcing stimuli; hence, under certain conditions, a collectively ordered state emerges from a complex dynamical system. Phase-locking occurs in STNOs because magnetic precession, the source of microwave oscillations, is inherently nonlinear[20].

Electrical nano-contacts to thin-film magnetic bilayer mesas are d.c. current-controlled STNOs that produce microwave precession ranging from 1 GHz to beyond 40 GHz, with spectral linewidths typically in the range 2–50 MHz at room temperature[6,21]. The oscillations are detected by measuring the time-varying voltage across the device caused by the giant magnetoresistance (GMR) effect[22] and the d.c. current through the contact. When active, the STNOs are predicted to generate spinwaves flowing outward from the region immediately beneath the nano-contact[23]. With the intent of using spinwave interactions to facilitate phase-locking between two STNOs, we investigated a device with two independently connected approximately 40-nm diameter contacts A and B separated by 500 nm on the same mesa (Fig. 1a, b). The two contacts are separately current biased, making each contact an independently controlled STNO. Bias-tees separate the d.c. current applied through each oscillator from the generated high-frequency output signal. The

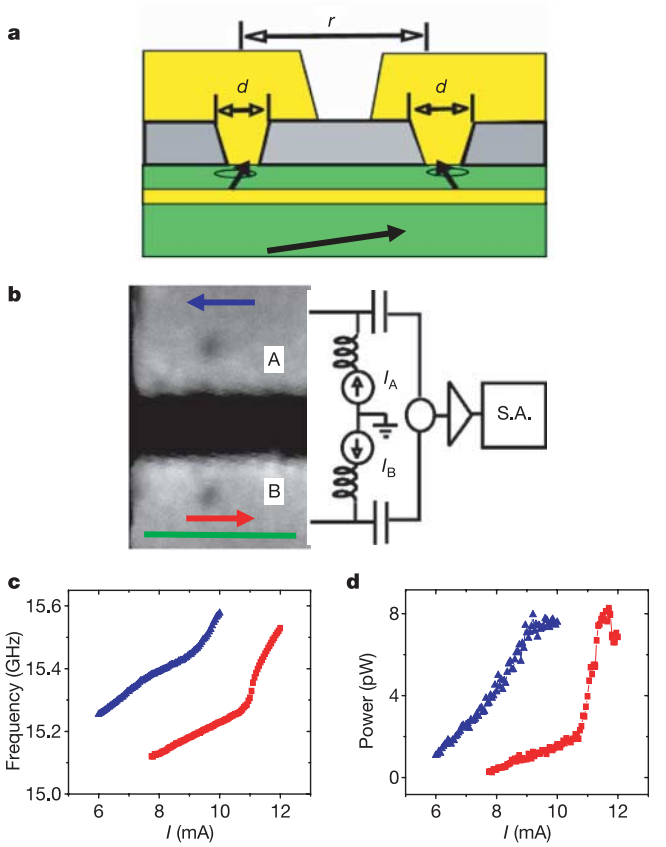


Figure 1 | Structure and basic behaviour of a two-nano-contact device. **a**, Cross-sectional diagram of a two-nano-contact device structure with contact diameter $d \approx 40$ nm and contact separation $r = 500$ nm on a single mesa. The mesa layer structure is [Ta 5 nm/Cu 50 nm/$Co_{90}Fe_{10}$ 20 nm/Cu 5 nm/$Ni_{80}Fe_{20}$ 5 nm/Cu 1.5 nm/Au 2.5 nm]. **b**, Micrograph of actual two-nano-contact device with two independent leads. Scale bar (green), 500 nm. the blue arrow gives the direction of the Ampere field generated by positive current (coming out of the plane) through contact B at contact A. The red arrow is the direction of the Ampere field generated by contact A at contact B and also the direction of the in-plane component of the external magnetic field. At the right is shown a measurement diagram showing a bias tee and d.c. current source for each contact. The high-frequency power output is combined in a microwave power combiner and then sent to the spectrum analyser (S.A.). **c**, Plot of frequency of non-interacting oscillator against current. The blue curve is output for contact A, the red curve for contact B. **d**, Plot of power output against current for each non-interacting oscillator; blue triangles are for contact A, red squares for contact B.

[1]Electromagnetic Technology Division, National Institute of Standards and Technology, Boulder, Colorado 80305, USA. [2]Hitachi San Jose Research Center, San Jose, California 95120, USA.

© 2005 Nature Publishing Group

output signals of both STNOs are sent to a microwave power combiner, and the combined signal is amplified and measured by a spectrum analyser (Fig. 1b). The amplifier gain has been divided out of all presented data. The electrical isolation between the contacts is −37 dB. Measurements are taken with the device placed in an external 740-mT magnetic field oriented 75° from the film plane.

The peak frequencies of each STNO, when biased alone (no current through the other contact), are shown in Fig. 1c. The frequencies exhibited by each oscillator agree with the behaviour of previously studied single-contact devices at the same applied field and field angle[21]. However, slight differences exist in the frequency and power output (Fig. 1d) for each oscillator. The frequency and power are determined from lorentzian fits to the peaks in the measured power spectral density (spectrum). According to the data in Fig. 1c, certain combinations of currents applied to both STNOs will result in coincidence of their respective oscillation frequencies.

When the frequency of one STNO is made to approach the other, interactions cause the oscillators to lock together. Figure 2a plots the evolution of the combined spectrum from both STNOs as current I_B through contact B increases. The current I_A through contact A is fixed at 8.0 mA. As I_B increases from 7 to 8.2 mA, only signal A (sourced by contact A) is visible. The frequency f_A of A decreases slightly with I_B owing to the Ampere field (about 3 mT to 5 mT) generated by I_B. This Ampere field opposes the in-plane component of the applied field and its direction is shown by the blue arrow in Fig. 1b. For 8.2 mA $< I_B <$ 9.2 mA, the signal from contact B appears and its frequency f_B increases towards f_A with the same slope as in the non-interacting case (Fig. 1c). The spectrum at $I_B = 8.65$ mA, shown in Fig. 2b, contains peaks from both STNOs. Above $I_B = 9.2$ mA, f_A suddenly unites with f_B until I_B exceeds about 11 mA. These data show that both STNOs frequency-lock over a 1.5-mA range in I_B, with the implication that signals A and B are also phase-locked. We give direct evidence below of phase-locking. The spectrum of the locked state at $I_B = 9.5$ mA (Fig. 2c) shows a single peak with much larger amplitude and a narrower linewidth than the peaks in Fig. 2b. For $I_B \geq 11$ mA, f_A and f_B separate and diverge. Figure 2d shows the spectrum of two peaks at $I_B = 11.5$ mA, where both peaks are weaker and broader than the locked state peak. Unlocking occurs at a sharp jump in f_B that is also seen in the non-interacting behaviour of B at 11 mA (Fig. 1c). Figure 2e plots the linewidths as a full-width at half-maximum (FWHM) for all peaks in the spectra. During locking, the FWHM decreases by about an order of magnitude to about 2 MHz.

Next we studied the individual output of each STNO as they evolved through the locking process (in contrast to their combined signal). Figure 3a shows the evolution of only signal A as I_B is tuned and I_A is fixed at 8.0 mA. In this measurement, the high-frequency output from B is disconnected from the power combiner and terminated into a 50-Ω load. The linewidth of A, shown by the

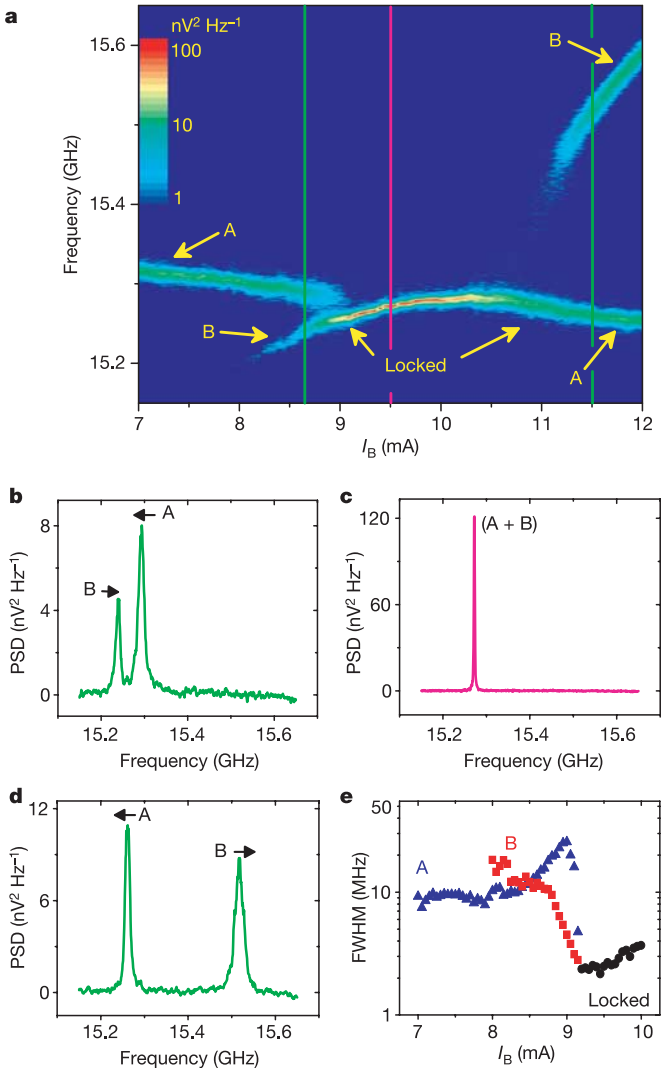


Figure 2 | Locking behaviour. **a**, Combined spectrum from both contacts as current through contact B is ramped from 7 mA to 12 mA. Current through contact A is fixed at 8 mA. Spectral intensity (colour) is a logarithmic scale. **b**, Spectrum (power spectral density; PSD) corresponding to the green vertical line in **a** at 8.65 mA. The arrows indicate the movement of the peaks as current through B increases. **c**, Spectrum corresponding to the magenta vertical line in **a** at 9.5 mA. **d**, Spectrum corresponding to the green vertical line in **a** at 11.5 mA. Arrows indicate motion of the peaks as current through contact B increases. **e**, Linewidths of combined output spectrum, where red squares correspond to the lower-frequency peak initially due to the signal from B, blue triangles correspond to the higher-frequency signal initially from A, and black circles correspond to the locked state. Uncertainty in the linewidth measurement is typically less than 0.75 MHz, which derives from one standard deviation to a lorentzian fit to the spectral peaks.

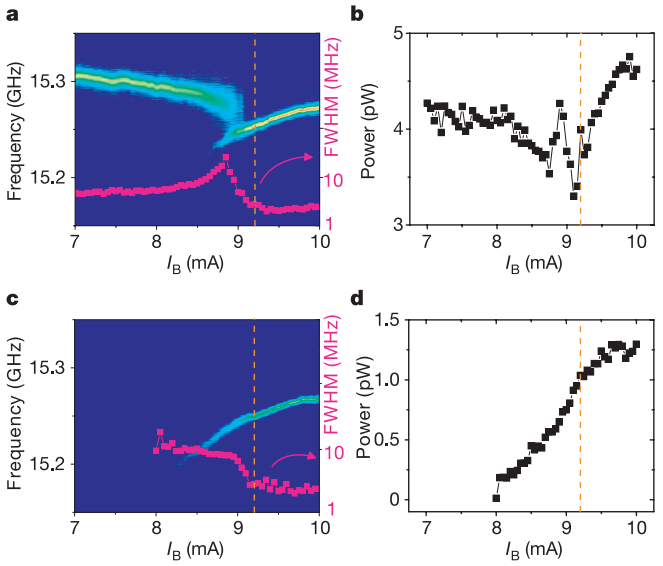


Figure 3 | Behaviour of individual oscillators. Dashed vertical lines (orange) denote the beginning of the locking range. **a**, Spectral intensity measured only for oscillator A as current through contact B is ramped and current through contact A is fixed at 8 mA. The colour scale is the same as for Fig. 2a. The superimposed magenta curve shows the linewidth of signal A on the same current scale. **b**, Power of oscillator A only. **c**, Spectral intensity measured only for oscillator B with the same currents through both contacts. The superimposed magenta curve shows the linewidth of signal B. **d**, Power of oscillator B only.

© 2005 Nature Publishing Group

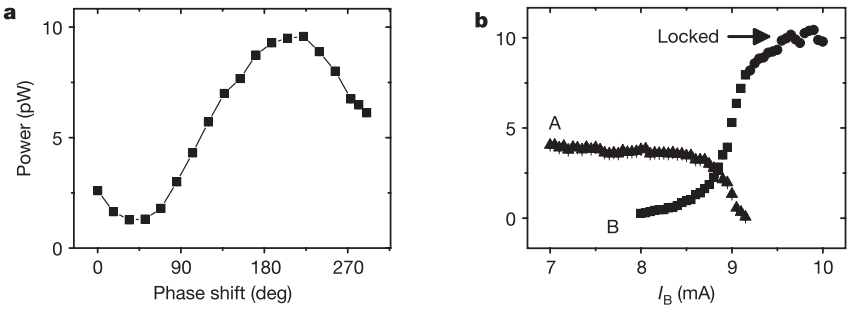


Figure 4 | Device power outputs. a, Power in the locked state as the phase of A is shifted. The current through contact A is 8 mA; the current through contact B is 9.55 mA. **b**, Measured power output for both oscillators as the current through contact B is ramped. The phase shifter is set for maximum output power (constructive interference) at 9.55 mA through contact B. Triangles indicate power in the higher-frequency signal initially due to oscillator A, squares indicate power in the lower-frequency peak initially due to B. Circles indicate power of the locked state. Uncertainty in the power measurement ranges from 0.01 to 0.1 pW and is determined from one standard deviation to a lorentzian fit to the measured spectral peaks.

magenta curve in Fig. 3a, narrows when the system locks. The power output of A (Fig. 3b) is constant until the system nears lock; on locking, the power from A increases. The evolution of only signal B is shown in Fig. 3c, and its power output is given in Fig. 3d. The current-dependent power from B is almost identical to the non-interacting case (Fig. 1d). The dissimilarity in the power of A and B remains even as the oscillators lock. The increase in power from A during locking is possibly caused by a change to a magnetization trajectory with higher GMR as oscillator A tracks to the locked frequencies. Although the power outputs of each STNO differ, both oscillators show narrowing to about the same linewidth of 2 MHz during locking. The abrupt decrease in linewidth indicates a reduced sensitivity to input noise (such as thermal fluctuations) for both oscillators because they provide mutual feedback when locked. Such an increased stability against frequency and phase fluctuations is also known for the synchronized generators of the North American power grid[13] and is predicted for arrays of Josephson junction oscillators[16].

The phase coherence of signals A and B during locking ($I_A = 8.0$ mA and $I_B = 9.55$ mA) is shown by varying the relative phase between the outputs of the STNOs. A phase-shifting element is placed in line with the cables carrying signal A to the combiner. By fully varying the phase shifter, the phase between the two signals at the combiner is adjusted over a range of about 300°, and this produces a sinusoidal variation in the combined output power corresponding to a change from destructive to constructive interference between signal A and B (Fig. 4a). Hence, a time-independent phase relationship between the signals must exist (phase-locking occurs). With the phase shifter set to maximize the amplitude at $I_B = 9.55$ mA and $I_A = 8.0$ mA, the combined output power from both oscillators is measured as I_B is ramped (Fig. 4b). The individual oscillator powers at $I_B = 9.55$ mA are $P_A = (4.37 \pm 0.03)$ pW and $P_B = (1.19 \pm 0.01)$ pW. The measured oscillator power is proportional to the square of the oscillating voltage waveform emitted by the STNO. If each oscillator were simply locked in frequency but incoherent in phase, the time-averaged total power output would simply be $P_A + P_B = (5.56 \pm 0.04)$ pW. However, the measured output power is $P_{total} = (9.90 \pm 0.07)$ pW (Fig. 4b), which is close to the expected power for two phase-coherent voltage waveforms that constructively interfere, $P_c = P_A + P_B + 2\sqrt{(P_A P_B)} = (10.15 \pm 0.05)$ pW.

STNOs have also been shown to phase-lock (injection lock) to fixed-frequency external sources, coupled by means of input microwave currents or external microwave magnetic fields[24]. In the system studied here, the interactions causing locking are mutual: either spinwave excitations[23] emitted by both oscillators or a.c. dipole magnetic-field interactions. Micromagnetic simulations[25] that incorporate a spin torque term derived by Slonczewski[1] show that large-amplitude spinwaves exist at a distance of 500 nm from the emitting nano-contact. Oscillating dipole fields, generated by localized precession underneath one contact, are estimated to be about 0.1 mT at the location of the other contact. Simulations predict this to be a sufficient field to induce locking. Moreover, a.c. magnetostatic fields caused by travelling spinwaves may exceed 10 mT at each contact, according to the micromagnetic simulations. The strength of both the spinwave and dipolar interactions, in principle, decays with the separation distance. Experimentally, for two STNOs separated by 1,000 nm, we find that although the frequencies of each oscillator can be made to intersect, weakened interactions result in no phase locking over a finite current for an applied field of 740 mT oriented 75° out of the film plane.

We have demonstrated phase-locking of two STNOs separated by 500 nm. Combined power in the phase-locked state is the coherent sum of the individual power of each oscillator. Hence, we anticipate that a phase-locked array of N STNOs can produce power that scales as N^2, leading to substantial narrowband power output (on the order of microwatts) generated from a micrometre-sized device at room temperature. A practical STNO-array device will probably require current from a single source distributed to each oscillator through parallel or series connections. These devices have applications as sources in nanometre-scale phased arrays, which could be used in wireless chip-to-chip or intra-chip communications.

Received 12 May; accepted 14 July 2005.

1. Slonczewski, J. C. Current-driven excitation of magnetic multilayers. *J. Magn. Magn. Mater.* **159,** L1–L7 (1996).
2. Berger, L. Emission of spin waves by a magnetic multilayer traversed by a current. *Phys. Rev. B* **54,** 9353–9358 (1996).
3. Katine, J. A., Albert, F. J., Buhrman, R. A., Myers, E. B. & Ralph, D. C. Current-driven magnetization reversal and spin wave excitations in Co/Cu/Co pillars. *Phys. Rev. Lett.* **84,** 4212–4215 (2000).
4. Tsoi, M. *et al.* Generation and detection of phase-coherent current-driven magnons in magnetic multilayers. *Nature* **406,** 46–48 (2000).
5. Kiselev, S. I. *et al.* Microwave oscillations of a nanomagnet driven by a spin-polarized current. *Nature* **425,** 380–383 (2003).
6. Rippard, W. H., Pufall, M. R., Kaka, S., Russek, S. E. & Silva, T. J. Direct-current induced dynamics in $Co_{90}Fe_{10}/Ni_{80}Fe_{20}$ point contacts. *Phys. Rev. Lett.* **92,** 27201 (2004).
7. Covington, M., Al Haj Darwish, M., Ding, Y., Gokemeijer, N. J. & Seigler, M. Current-induced magnetization dynamics in current perpendicular to the plane spin valves. *Phys. Rev. B* **69,** 184406 (2004).
8. Krivorotov, I. N. *et al.* Time domain measurements of nanomagnet dynamics driven by spin-transfer torques. *Science* **307,** 228–231 (2005).
9. Wolf, S. A. *et al.* Spintronics: a spin-based electronics vision for the future. *Science* **294,** 1488–1495 (2001).
10. Benz, S. P. & Burroughs, C. J. Coherent emission from two dimensional Josephson junction arrays. *Appl. Phys. Lett.* **58,** 2162–2164 (1991).
11. Wengler, M. J., Guan, B. & Track, E. K. 190-GHz radiation from a quasioptical Josephson junction array. *IEEE Trans. Microwave Theory Tech.* **43,** 984–988 (1995).
12. Popovic, Z. B., Weikle, R. M., Kim, M. & Rutledge, D. B. A 100-MESFET planar grid oscillator. *IEEE Microwave Theory Tech.* **39,** 193–200 (1991).
13. Strogatz, S. *Sync: The Emerging Science of Spontaneous Order* 51, 116 (Hyperion, New York, 2003).

© 2005 Nature Publishing Group

14. York, R. A. Nonlinear analysis of phase relationships in quasi-optical oscillator arrays. *IEEE Trans. Microwave Theory Tech.* **41,** 1799–1809 (1993).
15. Rezavi, B. A study of injection locking and pulling in oscillators. *IEEE J. Solid State Circuits* **39,** 1415–1424 (2004).
16. Wiesenfeld, K., Colet, P. & Strogatz, S. H. Synchronization transitions in a disordered Josephson series array. *Phys. Rev. Lett.* **76,** 404–407 (1996).
17. Finnegan, T. F. & Wahlsten, S. Observation of coherent microwave radiation emitted by coupled Josephson junctions. *Appl. Phys. Lett.* **21,** 541–544 (1972).
18. Buck, J. & Buck, E. Mechanism of rhythmic synchronous flashing of fireflies. *Science* **159,** 1319–1327 (1968).
19. Bennet, M., Schatz, M. F., Rockwood, H. & Wiesenfeld, K. Huygens's clocks. *Proc. R. Soc. Lond. A* **458,** 563–579 (2002).
20. Suhl, H. The nonlinear behaviour of ferrites at high microwave signal levels. *Proc. Inst. Radio Engrs.* **44,** 1270–1284 (1956).
21. Rippard, W. H., Pufall, M. R., Kaka, S., Silva, T. J. & Russek, S. E. Current-driven microwave dynamics in magnetic point contacts as a function of applied field angle. *Phys. Rev. B* **70,** 100406 (2004).
22. Baibich, M. N. *et al.* Giant magnetoresistance of (001)Fe/(001)Cr magnetic superlattices. *Phys. Rev. Lett.* **61,** 2472–2475 (1988).
23. Slonczewski, J. C. Excitation of spin waves by an electric current. *J. Magn. Magn. Mater.* **195,** L261–L268 (1999).
24. Rippard, W. H., Pufall, M. R., Kaka, S., Silva, T. J. & Russek, S. E. Injection locking and phase control of spin transfer oscillators. *Phys. Rev. Lett.* **95,** 067203 (2005).
25. Russek, S. E., McMichael, R. D., Donahue, M. J. & Kaka, S. in *Spin Dynamics in Confined Magnetic Structures II* (eds Hillebrands, B. & Ounadjela, K.) 93–156 (Springer, Berlin, 2003).

Acknowledgements We thank P. Kabos and A. Kos for assistance with microwave apparatus, and A. Slavin, M. Stiles, T. Gerrits and R. Goldfarb for discussions. This work was partly supported by the US government.

Author Information Reprints and permissions information is available at npg.nature.com/reprintsandpermissions. The authors declare no competing financial interests. Correspondence and requests for materials should be addressed to S.K. (shehzu21@gmail.com).

© 2005 Nature Publishing Group